DOI:10.31653/smf51.2025.138-150

Received 11.10.2025 Accepted 28.10.2025

Zhuravlov Yu.I., Korkh M. V

National University «Odessa Maritime Academy»

DEVELOPMENT OF A MODEL FOR THE DESTRUCTION PROCESS OF CRANKSHAFTS OF MARINE DIESEL ENGINES TAKING INTO ACCOUNT THEIR STRESS-STRAIN STATE

Formulation of the problem in general form.

Crankshaft quality issues include mechanical damage (scoring, chipping, scratches), geometric distortion (deformation, deflection, runout), and accelerated wear (of journals, bearings, and bores), which often leads to engine imbalance, increased noise and vibration, and ultimately, engine failure. These can be caused by manufacturing defects or operational errors, such as unscheduled oil changes, overheating, or excessive loads. Fatigue failure is the most common cause of crankshaft failure, especially in steel crankshafts, accounting for 70% of failures. This occurs due to repeated stress cycles, even when the stress is below the material's yield strength.

Cracks often form in high-stress areas of the crankshaft, such as the journal-to-journal joint [1]. These cracks can start small but grow over time, especially when the piston is at top dead center (TDC). As the engine continues to operate, cyclic loads can cause cracks to propagate, leading to complete failure. Excessive axial clearance in the crankshaft assembly can also lead to axial movement during engine operation. This movement increases stress concentration, which in turn can lead to cracks and premature failure [3].

Crankshaft failure can be directly related to bearing issues, such as improper bearing installation or worn bearings. If the bearing nuts are loose or the clearance between the shaft and axle is too large, the crankshaft will experience uneven loading, leading to premature fatigue.

Considering the above, improving the quality of remanufactured diesel engine crankshafts, taking into account their stress-strain state, remains a relevant problem.

Setting the task.

- 1. Develop a flat model of a crankshaft crank.
- 2. Consider the stress-strain state of a reconditioned large-size crank-shaft subjected to alternating loads.

- 3. Develop a model suitable for analyzing the failure process of crankshafts of low-power marine diesel engines.
- 4. Develop the force interaction between the cutting tool and the workpiece.

Analysis of recent research and publications.

An analysis of literary sources reveals a shortage of domestic technological support for the restoration and repair of large diesel engine crankshafts. Similar technologies exist globally, with the Gleason process, a common example of which is the application of metal coatings under a flux layer using two different wires [2]. The need for technological support for the restoration of domestic large-sized crankshafts underlies the relevance of this study.

Crankshaft analysis includes diagnostics for defects, such as wear, scratches, scoring, and runout, using magnetic particle and ultrasonic testing [4]. Compliance with technical requirements is also assessed, such as checking journal geometry (ovality, taper), and analyzing the causes of wear for subsequent shaft restoration using grinding or thread and keyway restoration methods.

Presentation of the main research material.

To analyze potential defects and predict crankshaft failure locations, it is necessary to examine the stress-strain state of a reconditioned large crankshaft subjected to alternating loads [5]. Most frequently, fatigue failure occurs along the cheek in the overlap zone of the connecting rod and main journals (Fig. 1), which for low-power marine engines is 27.5 mm at the nominal journal size.

When regrinding the main and connecting rod journals to the final repair size, the overlap is reduced by 2 mm (7.2%). Calculations show that the bending stress level increases by an average of 8% [8].



Figure 1 - Form of fatigue failure of the crankshaft along the cheek

The size of the load-bearing cross-section decreases significantly during operation due to the propagation of fatigue cracks from the origins (in this case, the fillets), as shown in Figure 1.

To analyze the force interaction between the crank and main journals in the overlap zone, a flat model was proposed, shown in Figure 2.

Here, Z is the resultant force transmitted from the connecting rods; Z_A and Z_B are the support reactions.

For simplicity, we consider only the right-hand side of the model, where $l_{\rm ch}$ is the web thickness; $l_{\rm m}$ is the main journal length; and p is the journal overlap. In the overlap zone, the solid metal is replaced by a fixed rod system consisting of rods 2-1, 2-4, and 3-4.

The rods themselves have hinge joints at the corresponding nodes and can only experience axial loads in the form of tensile or compressive forces. If we cut the rod system with line 1-1 and examine the right part (Fig. 3), we can determine the forces in the rods themselves.

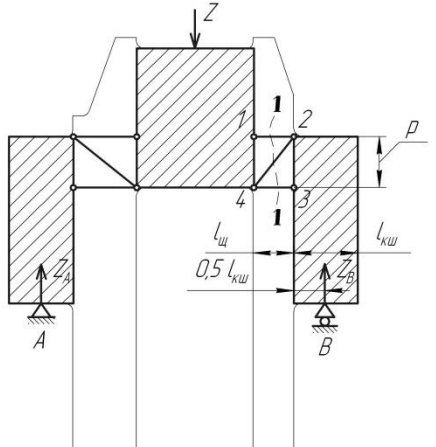


Figure 2 - Flat model of the crankshaft crank
Hence:

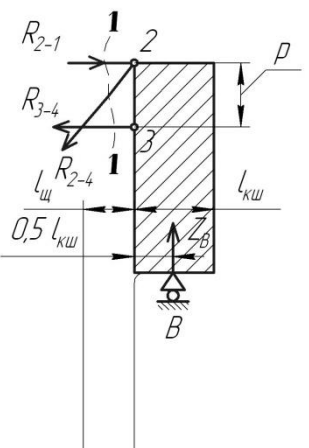


Figure 3 - Diagram for determining forces

$$R_{2-1} = \frac{Z_b \cdot \left(\frac{l_m}{2} + l_{ch}\right)}{p};$$
 (1)

$$R_{2-4} = \frac{Z_b \cdot \sqrt{p^2 + l_{ch}^2}}{p} \,; \tag{2}$$

$$R_{3-4} = \frac{Z_b \cdot \frac{l_m}{2}}{p} \,. \tag{3}$$

In formulas (1)-(3), R_{i-j} is the force transmitted by the rod, i -is the node to which the force is transmitted by the rod, and j -is the node from which this force is transmitted.

The top rod 2-1 will be compressed, while the other two -2-4 and 3-4 - will be stretched. Taking the overlap between the 4 main and crankpin journals of the engine as an example, 27 mm (including the over-chamfer flanges), 36 mm, and p = 27.5 mm, we obtain $R_{2-1} = 1.64$ Zb; $R_{2-4} = 1.40$ Zb; $R_{3-4} = 0.66$ Zb. It follows that the greatest tensile force is in rod 2-4 and is accompanied by a tensile force in rod 3-4, which constitutes 47% of the load in 2-4. Although the force in rod 2-1 exceeds the load in 2-4 by 17.1%, it is compressive and therefore we think it is not responsible for the failure of the component, and the hazardous section corresponds to the location of rod 2-4, which is clearly visible in the practical example (Fig. 1). Next, the geometry of the hazardous section was considered, with rod 2-4 serving as a model.

To develop a model suitable for analyzing the fracture process, a neck overlap diagram was considered (Fig. 4,a). Based on this, for the neck overlap value p, we have

$$p=R_{\kappa}+R_{uu}-r, \qquad (4)$$

where R_r is the radius of the main journal; R_c is the radius of the connecting rod journal; r is the radius of the crank.

For an engine crankshaft with a crank radius of 60 mm, a nominal diameter of the main journal of 95 mm and a connecting rod journal of 80 mm, the value of p corresponds to 27.5 mm, which was indicated above [6]. Next, the problem consisted of determining the coordinates of points B and C (the intersection points of the contours of the main and connecting rod journals) relative to the X and Y axes. Based on the rules of analytical geometry, relying on the equation of a circle, we obtain the coordinates of the points of the circumferences of the main and connecting rod journals [7]. Solving the system of equations for the above dimensions, we obtain the coordinates of the intersection points of the circumferences of the connecting rod and main journals (in mm) relative to the center of the main circle: B(-31,594; 35,469); C(31,594; 35,469). From here we calculate all the missing parameters of the circuit in Figure 4,a. Then:

$$a = 2 \cdot |x| = 63,188(mm),$$
 (5)

where a -is the chord of the overlap of the necks; x -is the value of the abscissa of point B or C.

To determine the main journal segment arrow h_k and the crank pin segment arrow h_c with the ordinate of the intersection points y, we use the following relationships:

$$h_{\kappa} = R_k - y = 12,031 \ (mm) \ ; \tag{6}$$

$$h_{u} = R_{u} - (r - y) = 15,469 \ (mm) \ .$$
 (7)

To determine the length of the overlap arc corresponding to the main journal lr and the length of the overlap arc corresponding to the crankpin l_k we use the values from (5-7) and the formula:

$$l_k = \sqrt{a^2 + \frac{16}{3} \cdot h_k^2} = 69,027(mm); \tag{8}$$

$$l_{uu} = \sqrt{a^2 + \frac{16}{3} \cdot h_{uu}^2} = 72,587(mm)$$
 (9)

It was assumed that these arcs represent the boundaries of the hazardous section along the guide line of the cylindrical surfaces of the journals. The length of the hazardous section 1 can be determined from Fig. 2 using the formula:

$$l = \sqrt{l_{ch}^2 + p^2} = 38,539(mm) \tag{10}$$

The numerical value here is defined for the web located between the 4th main journal and 4-th connecting rod journal of the engine crankshaft, taking into account the over-chamber flanges.

Thus, with some assumptions, the hazardous section can be represented as a flat model to which a tensile force is applied (Fig. 4, b).

The model is an isosceles trapezoid, the upper and lower bases of which are equal to the lengths of the support arcs l_{κ} and l_{ch} , calculated using formulas (8) and (9), and the height is equal to the value l, calculated using formula (10). The upper base has a distributed constraint along the Y-axis and is immobile along the X-axis. The lower base is loaded with a distributed (we assume uniformly distributed) load q, directed along the Y-axis, and the lower base is also immobile along the X-axis. The absence of displacements along the X-axis simulates the effect on the hazardous section of the remaining part of the jaw, including the counterweight, which is not subject to the loads under consideration [5].

When deriving an analytical description of the high-cycle fatigue curve, we assume that the failure intensity α_F increases directly proportionally to the actual amplitude of the acting stresses σ_{af} , that is,

$$\alpha_F = \frac{dF_p}{dN} = a\sigma_{af}, \tag{11}$$

where dF_P is the elementary small area of destruction for the number of cycles dN; a -is the proportionality coefficient characterizing the change in α_F per unit of stress amplitude $a = d\alpha_F/d\sigma_{afs}$.

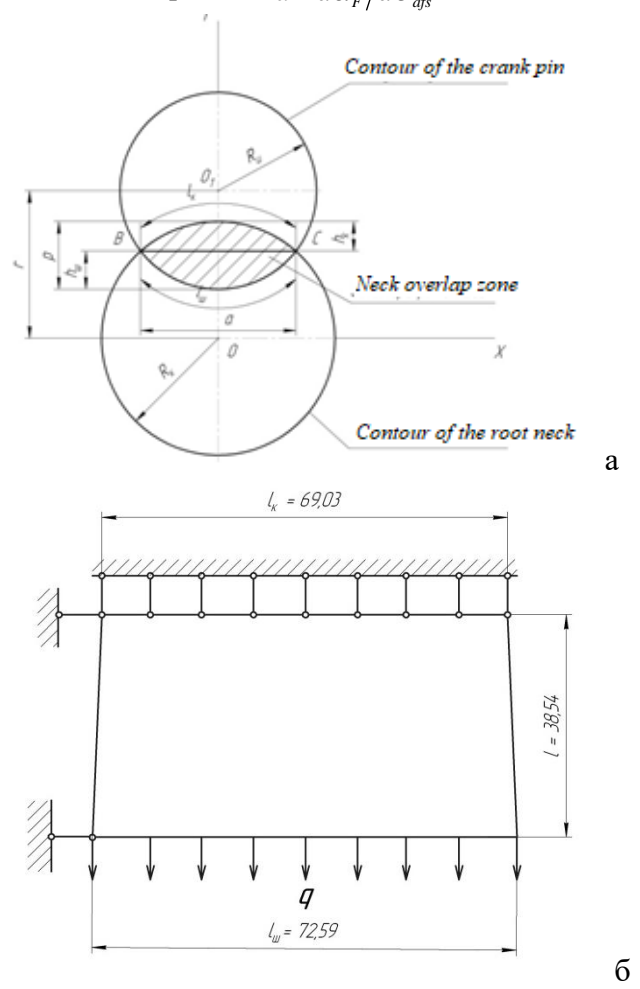


Figure 4 - a - diagram of the overlap of the crankshaft journals; b - a flat model of the dangerous section and a diagram of its loading

This assumption can be explained by Hooke's law, according to which, within the elastic limits, the deformation (leading to microplastic

failure) is directly proportional to the magnitude of the applied stress. Therefore, the dependence of σ_{af} on F_p , taking these factors into account, can be taken as the second assumption of linearity in the form

$$\sigma_{\rm af} = \sigma_a + cF_p \tag{12}$$

где $\sigma_a^{'} = \sigma_a - \sigma_{-1}$; c – proportionality coefficient characterizing the change in stress amplitude per unit area of destruction ($c = d\sigma_{at}/dF_p$).

Size σ_a is used as a free term due to the fact that fatigue failures begin to develop only under the condition $\sigma_a > \sigma_{-1}$, that is, when the amplitude exceeds the fatigue limit.

Taking into account dependence (12), differential equation (11) takes the form

$$\frac{dF_p}{dN} = a\sigma_a + acF_p. \tag{13}$$

Integration of the differential equation (13) under the initial conditions $F_p = 0$ at N = 0 allows us to obtain the dependence of the destruction area F_p on the number of cycles N, therefore, we can calculate the dependence of the actual stress amplitude σ_{af} on the number of loading cycles and, as a consequence, we can determine the total destruction area:

consequence, we can determine the total destruction area:
$$F = F_{p0} + F_p = F_{p0} + F_{p0} \left(e^{bN} - 1\right) = F_{p0} e^{bN}. \tag{14}$$

When improving crankshaft design and justifying restoration methods, it is necessary to consider the characteristics of fatigue failure. This primarily concerns the avoidance of cold straightening of shafts, which reduces fatigue strength by 30% or more. A network of microcracks in the die joint zone has a similar effect (by 20-40%). Roller knurling of fillets increases fatigue strength by 15%.

The main criterion for analysis in this area is the correspondence between the failure mode of the actual object and the predicted failure mode of the model. A crankshaft, welded under a layer of AN-348A flux using 1.6Np-30KhGSA wire, was ground (Fig. 5), and then operated under real conditions until failure. The destruction occurred in two places: across the fourth crank journal from the rear end of the part and in the area of the adjacent cheek from the front flange of the shaft (Fig. 6).

The classic loading scheme for calculating crankshaft strength is shown in Fig. 7. The calculated loads are the radial Z and tangential T (acting on an arm equal to the crank radius r), which are the components of the total forces. Accurately calculating the strength of a crankshaft is practically impossible due to the complexity of its shape. The crankshaft

is primarily calculated as a flat, two-support frame, one end of which rests on a movable hinge, and the other on a fixed one. Axial loads are absent in this case. A study of the causes of crankshaft failure shows that in most cases they are a consequence of material fatigue. Elements of the study are presented in Figs. 8 and 9.

The most dangerous sections of the crankshaft in this regard are those where significant stress concentrations can occur [4]. It is a priori known that the edges of the lubrication holes in the connecting rod and main journals are the critical points, while in the webs, the areas where they meet the journals are the critical points.

Practical experience in testing and operation shows that, in the ultimate state, the crankshaft typically fails as a result of normal stresses caused by bending loads in the crank plane.



Figure 5 - The fourth crankshaft journal before failure



Figure 6 - The nature of the destruction of the crankshaft journal as a result of its operation

Crankshafts exhibit the characteristic torsional failure pattern extremely rarely. Theoretically, the distribution of internal stresses in a crankshaft can be described using grid or variational calculation methods. The finite element method is a variational method [7].

Assumptions were made: first, a flat model was considered, with the outlines of a projection of a fragment of a real crankshaft onto a plane parallel to the crank plane; - secondly, due to the law:

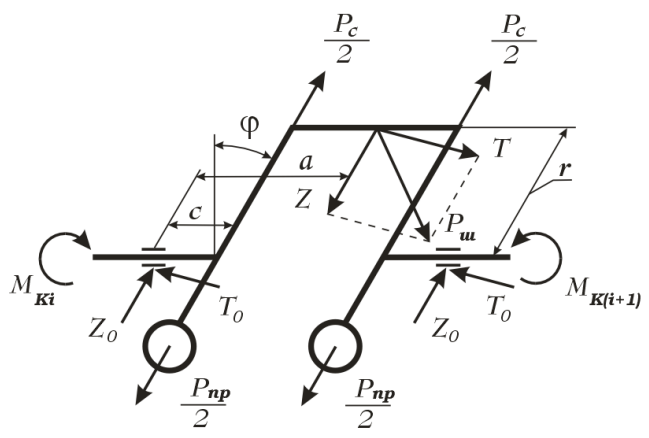


Figure 7 - Classic crankshaft design diagram

$$M_{b} = Z_{0}a - \left(\frac{P_{gi}}{2} - \frac{P_{c}}{2}\right)(a-c),$$
 (15)

where M_{b} is the magnitude of the bending moment, Z0 is the reaction of the support in the plane of the crank, is the distance from the support to the middle of the crank journal, P_{gi} -is the centrifugal force of inertia from the rotation of the counterweights, P_{c} - is the centrifugal force of inertia from the rotation of the crank, c- is the distance from the support to the shaft cheek, we neglect components P_{gi} and P_{c} , conventionally assuming that they balance each other;

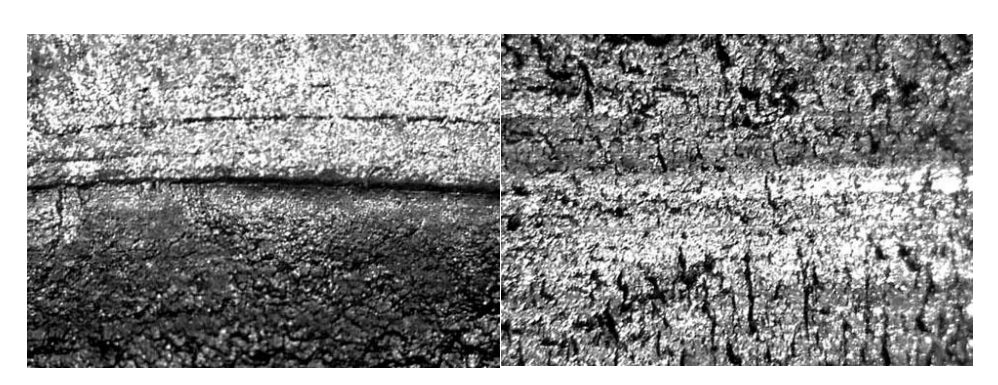


Figure 8 - Macrostructure of a cheek fracture: Transition from the fatigue crack development zone to the brittle fracture zone (50:1)

Figure 9 - Macrostructure of a transverse neck fracture: fatigue crack development zone (50:1)

- third, the load on the crank journal from the two connecting rods was replaced by a uniformly distributed load and equated to unity. The latter, within the limits of Hooke's law, does not lead to a change in the ratio of the internal stresses, therefore their distribution pattern in the part remains the same;
- fourth, given that the maximum load from the gas pressure is transmitted through the connecting rod at a crankshaft rotation angle ϕ equal to approximately 15° from the top dead center of the compression stroke, practically the entire load P_c , due to the smallness of this angle, is applied as a shear force to the crank journal, and the tangential component T is very small, as is T_0 . For the same reason, the incident M_{ru} and tail $M_{s(i+1)}$ torques were not considered.

Thus, a two-dimensional model was used (Fig. 10). Approximation was performed using triangular elements. The finite element breakdown is shown in Fig. 11. The diagram included 194 nodes, which was sufficient for visualizing the results [10].

The stress state was assessed using the von Mises criterion σ_e , for which the general formula is:

$$\sigma_{e} = \sqrt{\frac{1}{2} \left[\left(\sigma_{1} - \sigma_{2} \right)^{2} + \left(\sigma_{2} - \sigma_{3} \right)^{2} + \left(\sigma_{3} - \sigma_{1} \right)^{2} \right]}, \tag{16}$$

where σ_1 , σ_2 μ σ_3 – principal stresses, ordered in descending order. In this particular two-dimensional case under consideration, $\sigma_3 = 0$.

The calculation results are shown in Fig. 11.

In Fig. 6 a characteristic S-shaped region extending across the crank journal is visible on the right (from the rear end of the shaft). The location of the stress region to the left of the crank journal (from the front end of the shaft) is also close to the fracture profile shown in Fig. 6.

By reducing the resolution, it is possible to identify regions where significant stresses will occur.

Identification of these areas is necessary for fatigue crack investigations during crankshaft inspection, both during operation and repair [9]. This yields highly satisfactory results, similar to those discussed above.

All this makes crankshaft failure amenable to prediction and simple visualization. After the surfacing operation, mechanical surface treatment with a cutting tool is necessary.

The force interaction between the cutting tool and the workpiece is shown in Figure 11.

Support reactions when basing in the machine:

$$R_A = P_Z - R_B, (17)$$

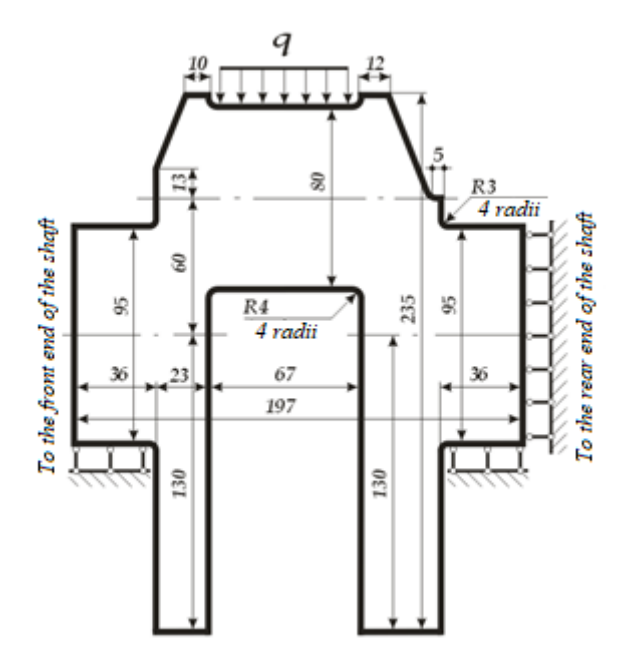


Figure 10 - Loading diagram of the fourth crank model of the engine crankshaft

where P_Z – tangential component of cutting force;

$$R_B = \frac{P_Z \cdot l_1}{l} \,, \tag{18}$$

where l_1 is the distance from the left support to the cutting zone; l -is the length of the workpiece.

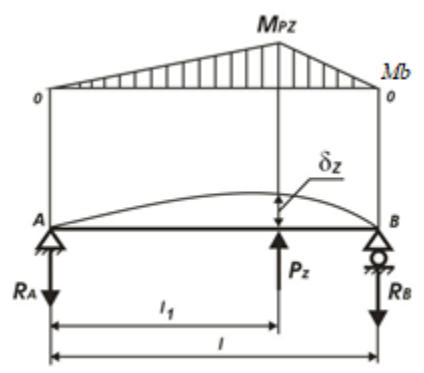


Figure 11 – Diagram of crankshaft loading of the tangential component of the cutting force during mechanical processing

Maximum bending moment M_{PZ} from the tangential component of the cutting force P_Z :

$$M_{PZ} = P_Z \cdot l_1 \cdot \left(1 - \frac{l_1}{l}\right) \tag{19}$$

Maximum bending moment M_{1Z} from unit force:

$$M_{1Z} = l_1 \cdot \left(1 - \frac{l_1}{l}\right). \tag{20}$$

Maximum deflection deformation δ_Z from the tangential component of the cutting force:

$$\delta_{Z} = \frac{1}{EJ} \cdot \left[\frac{1}{2} \cdot l_{1} \cdot M_{PZ} \cdot \frac{2}{3} \cdot l_{1} \cdot \left(1 - \frac{l_{1}}{l} \right) \right] + \frac{1}{EJ} \cdot \left[\frac{1}{2} \cdot \left(l - l_{1} \right) \cdot M_{PZ} \cdot \frac{2}{3} \cdot l_{1} \cdot \left(1 - \frac{l_{1}}{l} \right) \right],$$

where E -is Young's modulus; J -is the moment of inertia of the section of the part.

Conclusions and prospects for further research

- 1. Using the finite element method, two-dimensional physical and mathematical models of the crank were developed to determine internal stresses. The obtained calculation results confirmed the failure statistics of the actual component in operation. A unique crank model in the form of a rod system was also proposed, allowing for the calculation of the distribution of internal forces in the overlap zone of the connecting rod and main journals.
- 2. The macrostructure of the fracture in the cheek at the transition from the fatigue crack development zone to the brittle fracture zone and the macrostructure of the transverse journal fracture were obtained, illustrating the fatigue crack development zone.

References

- 1. Гоц О.М. Спосіб випробування колінчастого валу двигуна внутрішнього згоряння // Дизельні двигуни: зб. доповідей V національної наук.-техн. конф. Т. 2.
- 2. Гоц О.М. Метод розрахунку колінчастого валу за даними усталостних випробувань // Транспорт, екологія стійкий розвиток: Доповіді XII науково-технічна конференція з міжнародно участю. -Варна: Вид-во ТУ, 2016. Т. 13. С. 223-227.
- 3. Когаєв В.П. Розрахунки на міцність при напругах, змінних у часі/. -Львів: ЛСГА. 2023.-С. 343.

- 4. Барлоу Р., Прошан Ф. Статистична теорія надійності та випробування на безвідмовність. Київ: СО РАН, 2022, -С. 520.
- 5. Рябінін І. А. Надійність та безпека структурно-складних систем. Київ: Наука, 2024, С. 344,
- 6. Жиркін Ю.В.. Надійність, експлуатація та контакт деталей машин. — Київ, Техніка, 2019. — 168 с.
- 7. Ікрамов У.А.. Розрахункові методи оцінки абразивного зносу. .Львів: Малті-М. 2023.-С. 343.
- 8. Медведєв, С.Ф. Методи підвищення динамічної міцності сталевих деталей машин та конструкцій Київ: Наукова думка. 2021. 610 С.
- 9. Zienkiewicz, O.C. The Finite Element Method. Fifth Edition. V. 2. Solid Mechanics // O.C. Zienkiewicz, R.L. Taylor. Butterworth-Heinemann, 2020. 459 p.
- 10. Yamada, Y. Plastic stress-strain matrix and its application for the solution of elastic-plastic problems by the finite element method / Y. Yamada, N. Yoshimura, T. Sakurai // International Journal of Mechanical Sciences. 2018. V. 10. № 5. P. 343-354.